Check for updates

Chemistry–A European Journal
Research Article
doi.org/10.1002/chem.202401768
Chemistry Europe
European Chemical Societies Publishing
www.chemeurj.org

Hot Paper

Unravelling the Role of Structural Factors in the Luminescence Properties of Persulfurated Benzenes

Andrea Fermi,*[a] Simone D'Agostino,*[a] Yasi Dai,[a] Filippo Brunetti,[a] Fabrizia Negri,*[a] Marc Gingras,[b] and Paola Ceroni[a]

Room temperature phosphorescence rarely occurs from pure organic molecules, especially in the solid-state. A strategy for the design of highly emissive organic phosphors is still hard to predict, thus impeding the development of new functional materials with the desired optical properties. Herein, we analyze a family of alkyl and aryl-substituted persulfurated benzenes, the latter representing a class of organic solid-state triplet emitters able to show very high emission quantum yield at room temperature. In this work, we correlate structural parameters with the photophysical properties observed in different experimental conditions (diluted solution, crystalline and amorphous phase at RT and low temperature). Our results, corroborated by a detailed computational analysis, indicate a close relationship between the luminescence properties and i) the nature of the substituents on the persulfurated core, ii) the adopted conformations in the solid state, both in crystalline and amorphous phases. These factors contribute to characterize the lowest-energy lying excited-state, its deactivation pathways, the phosphorescence lifetime and quantum yield. These findings provide a useful roadmap for the development of highly performing purely organic solid-state emitters based on the persulfurated benzene platform.

Introduction

In recent years, increasing attention was devoted to organic and inorganic materials able to show room-temperature (RT) luminescence in the solid state,[1,2] because of their present and future applications in a vast area of optoelectronic technology for light generation. For instance, they include displays, organic light-emitting diodes (OLED) and luminescent sensors.[3,4] For such applications, several classes of compounds that show long-lived phosphorescence emission are the most attractive. In contrast to what is observed for many metal complexes with precious and rare metals, the efficient population of an emitting triplet excited state is often a challenge for pure organic materials, due to the absence of heavy atoms that can significantly affect spin-orbit coupling (SOC) and intersystem-crossing (ISC) rates.[5]

For this reason, the design of solid-state organic emitters showing RT phosphorescence with high quantum yields is considered crucial, along with an easy preparation on a large scale at reduced costs, compared to luminescent metal complexes based on rare metals. Several parameters are important such as: *i*) intra- or intermolecular interactions with functional groups displaying non-bonding electron pairs (*e.g.*, carbonyl,[6] cyano[7] groups, etc.) to increase ISC rates from singlet to triplet excited states ($S_n \rightarrow T_n$),[8] *ii*) functionalization with heavy atoms (e.g., Br, I) to facilitate SOC,[9,10] and *iii*) suppression of non-radiative deactivation pathways in order to increase the $T_1 \rightarrow S_0$ transition.[11,12] As for the latter, common solid-state fluorescence emitters (often named "molecular rotors" or "propellers") rely on the restricted bond rotations of aromatic substituents connected to a flat cyclic core, thus decreasing non-radiative deactivation exhibiting Aggregation Induced Emission (AIE)[13–16] at RT.[17–20] Such conformationally-restricted molecules can therefore be exploited in order to modulate their emissive behaviour according to the nature or conditions of their environment (*e.g.*, temperature,[21] solvent viscosity,[22] crystal packing,[23] polymorphism,[24] presence of intermolecular interactions in the solid state,[25] etc.).[26–30] As a consequence, the design of such organic materials with optimized properties must take into account several structural parameters.[31–33]

A clear understanding of the AIE mechanism for most organic molecules is far from being fully rationalized[34–36] and such challenge is one of the main goals of the analysis of the luminescence properties of persulfurated benzenes, such as hexakis-(arylthio)benzenes. The latter represent a class of pure organic triplet emitters with outstanding photophysical properties in the solid state, especially for their high emission quantum yield at RT: intense phosphorescence can be obtained from their crystals, coordination motifs, and in supramolecular complexes.[37–40] Some investigations are however needed in order to specify the role of chemical, structural and internal

[a] Dr. A. Fermi, Dr. S. D'Agostino, Dr. Y. Dai, F. Brunetti, Prof. Dr. F. Negri, Prof. Dr. P. Ceroni
Dipartimento di Chimica "Giacomo Ciamician"
Alma Mater Studiorum – Università di Bologna
Via Selmi 2, 40126 Bologna, Italy
E-mail: andrea.fermi2@unibo.it
simone.dagostino2@unibo.it
fabrizia.negri@unibo.it

[b] Prof. Dr. M. Gingras
Aix-Marseille Université, CNRS, CINaM,
163 Av. de Luminy, 13009 – Marseille, France

Supporting information for this article is available on the WWW under https://doi.org/10.1002/chem.202401768

© 2024 The Author(s). Chemistry - A European Journal published by Wiley-VCH GmbH. This is an open access article under the terms of the Creative Commons Attribution License, which permits use, distribution and reproduction in any medium, provided the original work is properly cited.

© 2024 The Author(s). Chemistry - A European Journal published by Wiley-VCH GmbH

geometrical factors of persulfurated arenes[41] (e.g.: presence of large or bulky substituents,[42] conformational symmetry,[43] non-covalent intermolecular interactions,[44] etc.).

Similar aspects have already been discussed for other classes of solid-state emitters based on the tetrakis-(arylthio)benzenes core.[45–49] Yet, a thorough description of the relationship between structural parameters and optical properties is unclear, especially those contributing to the enhancement of the phosphorescence quantum yield at RT.

In this work, we try to elucidate how changes in the excited state properties of persulfurated benzenes at the solid state can be correlated to both constitutional (nature of the substituents around the persulfurated core, presence of sterically hindered groups and their regiochemistry) and structural factors (e.g., conformational symmetry, core distortion, etc.). To achieve these goals, we considered a subset of persulfurated benzenes with aryl and alkyl substitutents (see Scheme 1) showing different conformations and arrangement in the solid phase. We then focused on the application of a variety of experimental conditions (namely temperature, solvation, and amorphization of the solid) to highlight their influence on key photophysical properties such as the emission profile, lifetime, and quantum yield. Our experimental and theoretical investigations disclose that the presence of aryl substituents on the persulfurated core is crucial to obtain phosphorescence at RT from crystalline phases, while their quantum yield is decisively dependent on conformation-related factors.

These aspects represent key features to be taken into account for future development of optical materials based on the persulfurated core and, in general, for RT emissive materials.

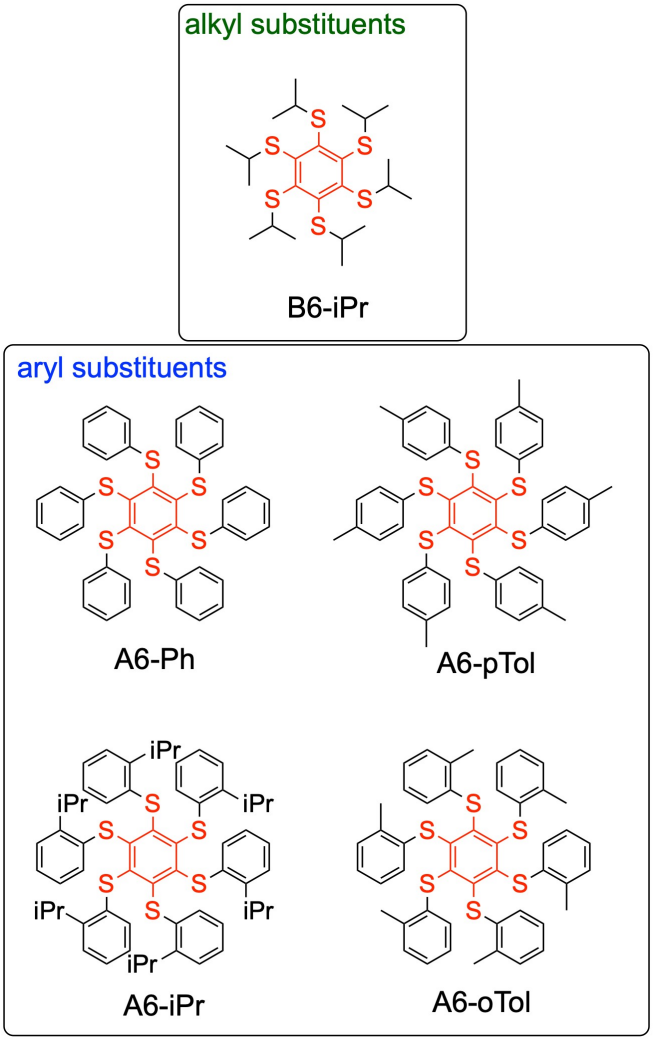

Scheme 1. Alkyl- and aryl-substituted persulfurated benzenes taken into account in this work.

Results and Discussion

Synthetic Procedures

Persulfurated benzene compounds can be prepared in a one-step sythesis, comprising numerous consecutive aromatic nucleophilic substitutions onto perhalogenobenzenes in polar aprotic solvents (usually DMF). Both alkyl- and aryl-thiols can be conveniently used for the generation of their corresponding thiolate salts the presence of a strong base (*e.g.* alkali metal carbonates, *t*-BuOK, or NaH). The synthetic procedures for all compounds in Scheme 1 are known and reported elsewhere. See also the Supporting Information (SI) for pertinent literature.[41,42,50,51]

Structural Characterization

The analysis and comparison of the molecular conformation and packing in the solid state for the two subsets of compounds have been carried out from their crystal structures, some of which have been previously determined by single-crystal X-ray diffraction (sc-XRD).[42]

Crystals of compounds **B6-iPr** suitable for sc-XRD were readily obtained from a slow evaporation of $CHCl_3$ solutions. Structural analysis confirms the molecular structure and that it crystallizes as a non-solvated structure, in the triclinic P-1 space group. As shown in Figure 1, the six isopropylthio-substituents bound to the central benzene core adopt an alternating *ababab* pattern (*a* and *b*: respectively, above and below the plane of the central ring),[41] as previously reported for **A6-Ph** and **A6-pTol**.[42] This is in contrast to what is observed in the crystal

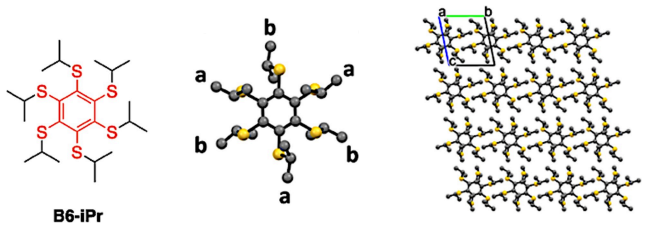

Figure 1. Molecular structure and corresponding packing diagram for **B6-iPr**, as determined from sc-XRD structural analysis showing the conformation (a and b for above and below the plane of the central benzene ring, respectively) of the six substituents bound to the central benzene core. H_{CH} omitted for clarity.

© 2024 The Author(s). Chemistry - A European Journal published by Wiley-VCH GmbH

15213765, 2024, 43, Downloaded from https://chemistry-europe.onlinelibrary.wiley.com/doi/10.1002/chem.202401768 by Area Sistemi Dipart & Doc, Wiley Online Library on [25/03/2025]. See the Terms and Conditions (https://onlinelibrary.wiley.com/terms-and-conditions) on Wiley Online Library for rules of use; OA articles are governed by the applicable Creative Commons License

structure of the analogue compound with six methyl susbstituents on the benzene core.[52] Depending on their conformation, the persulfurated benzenes examined here show significant differences in the torsion angles of the benzene core, which is mostly flat for highly symmetrical conformers (e.g., **B6-iPr** and **A6-Ph**), but more distorted for less symmetric ones, such as for **A6-oTol** (see Table 1 and Figure S5, SI). For the latter, it follows that peripheral S atoms are not in the in-plane positions compared to the benzene core, but torsion angles up to ca. 17° are evidenced for adjacent dihedral SC–CS bonds. Notably, similarly distorted persulfurated benzene structures are obtained from DFT optimized geometries in vacuo (see Table 1), demonstrating that the core distortions are mainly associated to specific conformers, rather than to their arrangement when immersed in a crystalline environment.

No specific intermolecular interactions are observed in the lattice of **B6-iPr**; crystal cohesion is due to dispersion forces in all cases, with molecules mainly by shape factor,[53] *i.e.* interlocking themselves in a columnar fashion. Comparing crystal structures of **B6-iPr** and the **A6**- derivatives, the π-systems of the central sulfurated rings cannot stack over each other efficiently due to high steric hindrance of the substituents. Thus, the interplanar distances between the central benzene rings are included between 8.1 and 15.1 Å (see Table 1).

Forming piles along the *a*-axis (see Figure 1), **B6-iPr** molecules exhibit crystallographic disorder for all six peripheral alkyl groups at RT, in contrast to what is observed for the **A6**- derivatives; this phenomenon can be related to the rotational motion of the isopropyl groups between two positions around the carbon-sulfur bonds, with occupations ranging from 30 to 60 %.

Upon decreasing the temperature to 110 K, this disorder could be partially solved, and the ordering of four isopropyl groups out of six is observed.

This behavior indicates that one of the partially occupied sites at RT becomes more stable and fully populated at 110 K, thus supporting a dynamic disorder model.[54] On the other hand, at 110 K the remaining two isopropyl groups are still disordered and, taking into consideration their thermal ellipsoids, this phenomenon can be better defined as a "continuous positional disorder".[54] The disorder observed for all six alkylthio substituents is restored when the crystal is warmed back to RT (see Figure 2).

Temperature-dependent structural analysis on crystalline and amorphous samples. With the aim of exploring the relationship between conformational flexibility of the compounds and their properties, variable temperature X-Ray diffraction (VT-XRD) on solid samples of **A6**- derivatives have been carried out, based on differential scanning calorimetry (DSC) measurements (see Figures S6–10). **A6-Ph**, **A6-pTol** and **A6-oTol** share a common and predictable structural behavior upon increasing temperature (Figure 3): the crystal structure at RT is lost when the samples reach the corresponding melting point. Amorphous phases are then produced by fast cooling in liquid N_2 of the melted phases. In addition, the original crystalline phases are obtained either by slow cooling of the melted compounds or by heating the amorphous phases below their melting points, which favours the structural reorganization. These findings are in agreement with the observed DSC traces of crystalline and amorphous samples of these compounds (see Figures S6–10, SI). Globally, the results indicate that the formation of different polymorphs is not observed in these experimental conditions and the three **A6**- derivatives showed in Figure 3 can recrystallize back to the original crystal structure even upon slow heating of the frozen amorphous phase from low temperature (77 K) to RT.

Table 1. Core conformations, core-core distances and maximum dihedral torsion angles (core CC–CC *vs.* peripheral SC–CS adjacent bonds) determined from sc-XRD of the crystal structures of persulfurated benzenes. Computed dihedral torsion angles are also reported for comparison.

Compound	C_6S_6 core conformation	Core-to-core distances in crystals (Å)	Max. dihedral torsion angles (core/periphery, °)	Computed max. dihedral torsion angles (core/periphery, °)[a]
B6-iPr	*ababab*	8.4	3.8/8.4	0.5/5.0
A6-Ph	*ababab*	10.3	3.5/2.1	4.5/5.6
A6-pTol	*ababab*	8.1	0.5/8.5	4.9/7.8
A6-oTol	*aaabbb*	15.1[b]	4.4/17.1	1.6/10.5[c]
	aabbab	15.1[b]	14.3/9.2	12.1/8.4[c]
A6-iPr	*aabaab*	11.6	9.6/10.6	10.6/9.3[c]

[a] From M06-2X/def2SVP + D3 calculations on isolated molecules. [b] Distances determined between two conformers of the same kind. [c] Optimized geometry of the *aaabbb*, *aabbab* and *aabaab* conformers of **A6-Ph**.

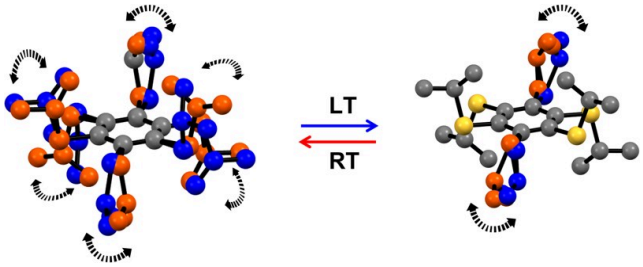

Figure 2. Representation of the flipping motion affecting the isopropyl groups in **B6-iPr** induced by temperature variations (LT = 110 K; RT = 300 K). H_{CH} atoms are omitted for clarity.

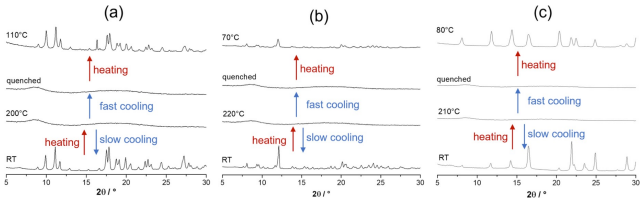

Figure 3. VT-XRD patterns from solid **A6-Ph** (a), **A6-oTol** (b) and **A6-pTol** (c) in different experimental conditions. Bottom to top: crystalline phases (RT), melted samples (200-220 °C), amorphous phases at low temperature (77 K), crystalline phase generated from heating of the amorphous phase (70–110 °C).

© 2024 The Author(s). Chemistry - A European Journal published by Wiley-VCH GmbH

15213765, 2024, 43, Downloaded from https://chemistry-europe.onlinelibrary.wiley.com/doi/10.1002/chem.202401768 by Area Sistemi Dipart & Doc, Wiley Online Library on [25/03/2025]. See the Terms and Conditions (https://onlinelibrary.wiley.com/terms-and-conditions) on Wiley Online Library for rules of use; OA articles are governed by the applicable Creative Commons License

15213765, 2024, 43, Downloaded from https://chemistry-europe.onlinelibrary.wiley.com/doi/10.1002/chem.202401768 by Area Sistemi Dipart & Doc, Wiley Online Library on [25/03/2025]. See the Terms and Conditions (https://onlinelibrary.wiley.com/terms-and-conditions) on Wiley Online Library for rules of use; OA articles are governed by the applicable Creative Commons License

Table 2. Photophysical data of persulfurated benzenes derivatives.

	Absorption		Emission						
	Solution RT		Solution RT	Rigid matrix 77 K			Crystals RT		
	λ_{onset} (nm)	λ (nm) / ε ($M^{-1}cm^{-1}$)		λ_{max} (nm)	τ (ms)	Φ_{em}	λ_{max} (nm)	τ (μs)	Φ_{em}
B6-iPr	420	291/18200	*not luminescent*	558	2.9, 7.9[b]	0.4	*not luminescent*		
A6-Ph	457	323/19300[a]	*not luminescent*	502[a]	3.6[a]	1.0	515	12.1[a]	1.0
A6-pTol	455	328/19400[a]	*not luminescent*	505[a]	4.0[a]	1.0	517	3.0[a]	1.0[a]
A6-oTol	463	316/20200[a]	*not luminescent*	509[a]	6.2[a]	1.0	519	15.8[a]	0.5[a]
A6-iPr	452	328/21600[a]	*not luminescent*	512[a]	8.9[a]	1.0	516	5.3[a]	0.06[a]

[a] Data from reference 42. [b] Biexponential fitting.

Photophysical Characterization

Key photophysical data for **B6-iPr** and **A6**- derivatives are gathered in Table 2. As generally observed for phenylthio-substituted benzenes,[37,39,42] the absorption spectra of **A6**- derivatives in CH_2Cl_2 show a broad band with maxima at ca. 320 nm and molar absorption coefficients around 2.0×10^4 $M^{-1}cm^{-1}$, not significantly affected by the presence of any of the selected alkyl substituents on the peripheral aromatic rings (Figure 4A). Solutions of all examined compounds are not emissive in solution at RT even upon oxygen removal, while intense phosphorescence (Φ_{em} ca. 100%) is observed from diluted rigid matrices at 77 K (Figure 4C). Most importantly, **A6**- derivatives display intense room-temperature phosphorescence in the crystalline phase (Figure 4B), with remarkable differences in quantum yields (from ca. 100% for **A6-pTol** and **A6-Ph** down to 6% for **A6-iPr**). The emission profiles and maxima recorded from solid phases at RT and from rigid matrices at 77 K are substantially unaffected by the nature and the position of the peripheral aliphatic substituents.[37,42] In both conditions, no fluorescence emission has been observed (see Figure S17–S22, SI). It is worth noting that compound **B6-iPr** is not displaying emission at RT, while phosphorescence has been detected at low temperature in rigid matrix (λ_{max} = 558 nm) and in the solid state at 77 K (see also Figure S11 and Table S2, SI).

Within the **A6**- family, the comparison between the luminescence properties indicates that: i) the substitution pattern has negligible effects on the energy of the lowest electronic transition and ii) different aryl substituents provoke dramatic effects on the emission quantum yield in solid state at RT, but not in rigid matrix at 77 K.

Therefore, for solid-state **A6**- derivatives, phenyl rings strain and intramolecular distortions strongly affect the interplay between radiative and non-radiative deactivation of the triplet excited states. On the other hand, in rigid matrix at 77 K, structural flexibility is strongly reduced and the radiative process represents the only deactivation pathway for the triplet excited state.

Luminescence properties in amorphous phases of A6-derivatives. To shed further light on the solid phase emission of **A6**- compounds and on the importance of the crystalline packing, we compared the behavior of the crystals at RT with the luminescence detected on annealed amorphous phases of the compounds at RT and at 77 K. Amorphous solids of **A6**-derivatives have been prepared by melting their powders (or crystals) in a glass pipette and quickly freezing them in liquid N_2. The so-obtained amorphous phases (see XRD data in Figure 3) display an unexpected red-shifted phosphorescence at 77 K (λ_{max} between 570 and 590 nm) in comparison to the corresponding crystalline phases at the same temperature (see Table 3 and Figure 5). The detected lifetimes, in the order of 10^{-3} s, indicate triplet excited state deactivations, while no fluorescence has been detected.

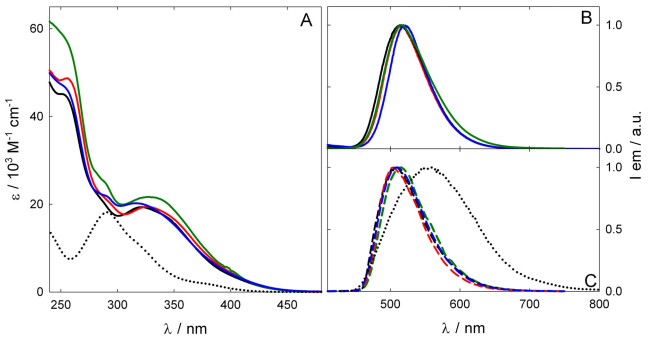

Figure 4. A: absorption spectra in CH_2Cl_2 at RT of compounds **B6-iPr** (dotted line), **A6-Ph** (black line), **A6-pTol** (red line), **A6-oTol** (blue line), and **A6-iPr** (green line). B: normalized emission spectra of solid samples at RT of the same compounds shown in A, except **B6-iPr** (λ_{ex} = 340–360 nm). C: normalized emission spectra of solid samples in CH_2Cl_2:CH_3OH rigid matrix at 77 K of the same compounds shown in A (λ_{ex} = 330–350 nm).

Table 3. Photophysical data of amorphous phases at 77 K.

Compound	λ_{max} (nm)	τ (ms)	Φ_{em}
A6-Ph	591	0.1, 6.0[a]	0.5
A6-pTol	589	6.3	0.6
A6-oTol	581	0.6, 5.8[a]	0.4
A6-iPr	577	5.1	0.5

[a] Biexpoential fitting.

© 2024 The Author(s). Chemistry - A European Journal published by Wiley-VCH GmbH

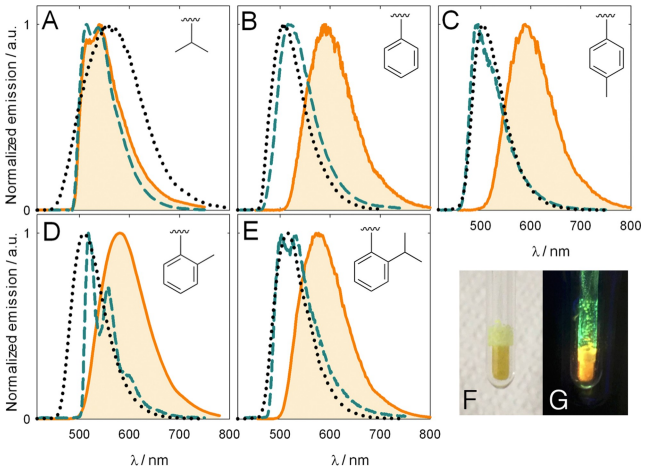

Figure 5. Comparison between normalized emission spectra of **A6**- derivatives (B–E) recorded in solid phases at 77 K (green lines), rigid matrix at 77 K (CH_2Cl_2:CH_3OH 1:1 v/v, black dotted lines) and solid amorphous phases at 77 K (orange lines; samples of **B6-iPr** prepared with the same procedure are also shown in A). $340 < \lambda_{ex} < 390$ nm. Pictures of amorphous samples of **A6-Ph** at RT under ambient light (F) and at 77 K with UV-excitation (G) are also shown.

We underline that for amorphous samples the phosphorescence is turned off at RT (estimated Φ_{em} at RT < 0.01), pointing out that the restrictions of intramolecular vibrations and rotation of bonds at low temperature are crucial to induce phosphorescence both in diluted frozen solutions and in the amorphous phase of the pristine compounds.

The highly intense phosphorescence of **A6-Ph** is restored upon slow crystallization of the sample (see Figure S14, SI), which comes to completeness after several hours, in agreement with VT-XRD experiments. Similar observations are found for **A6-pTol**, with a faster recovery of the corresponding phosphorescence (see Figure S15, SI). We can conclude that the phosphorescence energies of pure **A6**- derivatives at 77 K are strongly affected by the crystallinity of the sample, highlighting the correlation between excited states energies and structural distortions induced by amorphization.

Modelling Photophysical Properties of Persulfurated Benzene Derivatives

To uncover the interplay between intra- and intermolecular structural effects and photophysical properties, we first investigated the properties of an isolated molecule, and then assessed the effects of the environment via QM/MM calculations of the excited state properties.

B6-iPr and **A6**-derivatives with different peripheral substituents are characterized by a remarkable conformational freedom. It is therefore convenient to distinguish between rotations around S–C bonds in which the carbon atom belongs to the central persulfurated benzene core (hereafter labelled S–$C_{central}$) and around S–C bonds in which the carbon atom belongs to the aryl substituents (labelled S–C_{aryl}). Rotation around the former determines interconversion between conformers around the central persulfurated benzene core (for example from *ababab* to *aaabab*), while the latter rotation leads to different orientations of aryl substituents. Notably, the rotation around S–$C_{central}$ bonds is associated with remarkable molecular volume change, while rotation around S–C_{aryl} bonds is more volume conserving.

Role of core-substitution and conformation of the persulfurated benzene core. Previous computational investigations on similar compounds revealed a relevant role of the persulfurated benzene conformation on the photophysical properties,[37,43] demonstrating the dependence between the luminescence properties at the solid state and structural parameters, as suggested by our experimental data discussed above (Tables 1 and 2). Thus, we investigated the lowest-lying triplet excited electronic states to decipher *i*) the effect of replacing alkyl with aryl substituents (**B6-** versus **A6-** derivatives) and *ii*) the effect of core conformation by focusing on five different conformers of **A6-Ph**, taken as a model molecule (*ababab*, *aaabbb*, *aabaab*, *aaabab* and *aabbab*).

We start our discussion with the smallest investigated compound, **B6-iPr**, considering the *ababab* conformation found in the crystal. Two lowest triplet excited states, featuring different orbital nature, were optimized: one can be identified as dominated by the nπ* character while the other is identified as a ππ*, focusing on the orbital shape on the central benzene core. Note that such labels will be adopted for simplicity also for **A6-** derivatives, although the orbital nature can be strongly mixed for such larger derivatives.

Notably, a shallow minimum for the ππ* state can be found only under symmetry constraint (Figure S31, SI), which is however much closer to S_0 than the nπ* triplet, owing to its distorted core.[43] By relaxing all symmetry constraints, geometry optimization of the lowest triplet state leads to a crossing with the ground state, most likely representing a conical intersection (CI) seam. Based on the above, a schematic representation of the potential energy profiles (PEP) of the ground and of the two lowest triplet states (Figure 6) can explain the lack of luminescence from **B6-iPr** at RT: the initial population of the nπ* triplet will be followed by fast internal conversion to the lowest ππ* triplet state, with a quenching of the luminescence due to the T_1-S_0 CI.

The rigid environment provided both by the CH_2Cl_2:CH_3OH matrix or by the crystal at 77 K is expected to restrict the internal rotation of isopropyl substituents and stabilize the shallow minimum in the lowest ππ* triplet, due to the rigidochromic effect[55,56] (see Figure S31, SI): these two factors could prevent the access to the CI. In this case phosphorescence will compete with non-radiative T_1-S_0 decay, which can explain the observed Φ_{em} (Table 2). Conversely, the absence of luminescence in the crystal at RT can be attributed to the increased vibrational motion of the isopropyl substituents, as demonstrated by the observed crystallographic disorder.

In contrast to **B6-iPr**, the symmetric *ababab* conformer of **A6-Ph**, found in crystals of several **A6-** derivatives (Table 1), features a lowest triplet state of nπ* character, with the ππ* triplet state slightly above (Figure 7). A similar excited triplet state sequence, involving phosphorescence from the lowest nπ*

© 2024 The Author(s). Chemistry - A European Journal published by Wiley-VCH GmbH

15213765, 2024, 43, Downloaded from https://chemistry-europe.onlinelibrary.wiley.com/doi/10.1002/chem.202401768 by Area Sistemi Dipart & Doc, Wiley Online Library on [25/03/2025]. See the Terms and Conditions (https://onlinelibrary.wiley.com/terms-and-conditions) on Wiley Online Library for rules of use; OA articles are governed by the applicable Creative Commons License

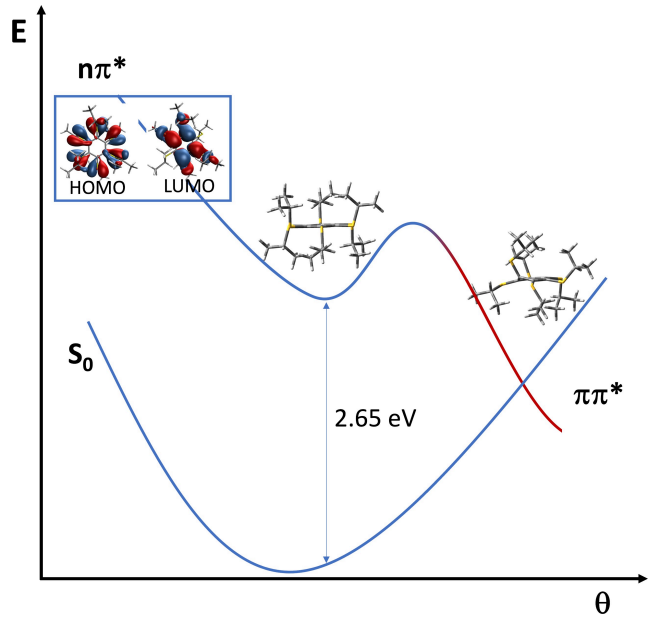

Figure 6. B6-iPr *ababab* conformer: schematic representation of the potential energy profiles of the two lowest triplet excited states (TD-M06-2X/def2-SVP + D3) and of the ground state (M06-2X/def2-SVP + D3) leading to lack of luminescence in solution RT. Θ is a displacement coordinate representing the multidimensional distortion of the central core as evidenced by the two optimized structures (the triplet minimum and T_1/S_0 crossing point).

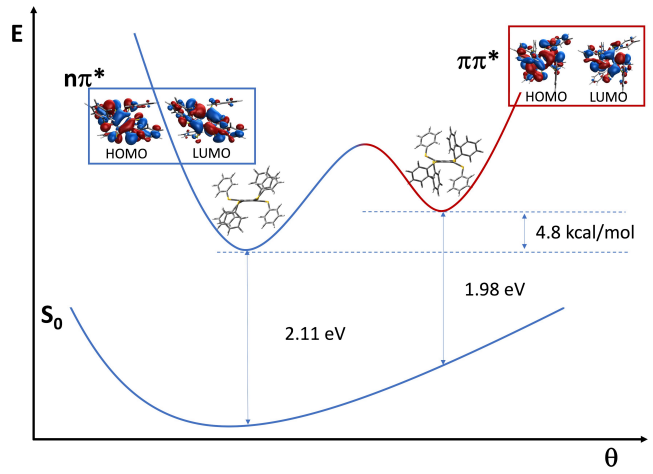

Figure 7. A6-Ph *ababab* conformer: schematic representation of the potential energy profiles of the two lowest triplet excited states (TD-M06-2X/def2-SVP + D3) and of the ground state (M06-2X/def2-SVP + D3) leading to efficient luminescence at RT. Θ is a displacement coordinate representing the multidimensional distortion of the central core as evidenced by the two optimized structures.

state, was found in previous works[37,43] using the CAM-B3LYP functional. Such uniform description, independent of the functional, combined with a negligible T_1-S_0 SOC at the symmetric triplet state geometry (Table S3, SI), strongly supports the efficient luminescence of crystals made by *ababab* conformers.

Rather than exploring different substituents for **A6-** derivatives, we investigated the lowest excited triplet states of different conformers of **A6-Ph** as a model compound, since our experimental results and previous investigations on similar molecules[47] demonstrate that the adopted conformation in the crystalline solid is a major factor determining the efficiency of phosphorescence. Before considering the additional conformers (beside *ababab*) found in our crystalline structures, we gauged the results of our calculations (carried out using the M06-2X functional) on the *aaabab* conformer, previously investigated using the CAM-B3LYP functional.[43] The computed PEPs (Figure S32, SI) for the lowest triplet states provide an interpretation of the deactivation processes, consistent with previous investigations. The computed lowest triplet state displays a mixed orbital nature but, due to the dominant contribution of the central benzene core in both HOMO and LUMO, is identified as a ππ*. Such state is found to cross the S_0 state, suggesting a CI seam as implied by previous CAM-B3LYP predictions and nicely validating the previously reported decrease in the luminescence quantum yield for crystals containing this conformer at RT.[43] A similar excited state pattern was determined for a different 4*a*,2*b* conformer (*aabaab*) that we found in the crystal of weakly emitting **A6-iPr** (Figure S33, SI). In such case, we could only determine one lowest triplet minimum, with dominant ππ* character, associated with a small T_1-S_0 energy difference that, combined with a large SOC of ca. 24 cm^{-1} (Table S3, SI), accounts for the quenched luminescence observed for the crystal at RT ($\Phi_{em} = 0.06$, see Table 2).

As shown in Table 1, two conformers are found in the crystal structure of **A6-oTol**. For the *aaabbb* conformer, we could only determine the optimized geometry of the nπ* triplet state which was found as the only lowest triplet state (Figure S34, SI) starting from different initial geometries. The SOC computed for the optimized structure of this conformer is negligible (Table S3, SI), suggesting efficient phosphorescence in crystals or rigid matrices. In contrast, the PEPs of the second conformer (*aabbab*) resembles very closely those of typical non-phosphorescent persulfurated benzene conformers such as the *aaabab* discussed above, showing evidence of a CI seam between T_1 and S_0 (Figure S35, SI). Thus, the reduced luminescence efficiency of **A6-oTol** ($\Phi_{em} = 0.5$, see Table 2) can be rationalized by considering the coexistence of highly phosphorescent and dark conformers in the same crystal. To summarize, the different stability of nπ* and ππ* states is influenced by substituents (alkyl vs. aryl) and by the conformations around the core. The latter strongly affects the planarity of the persulfurated benzene, such that less distorted core conformations (for instance *ababab* and *aaabbb*) stabilize the nπ* state with respect to the more distorted ππ* state, thus favoring radiative deactivation.

Effect of the environment on excitation energies and excited state relaxation. In this section we seek to uncover the role of environment and provide some insights on the emission at 77 K of the amorphous phases obtained from **A6-** derivatives, significantly red-shifted when compared to that detected from the corresponding crystals at RT.

Quantum-chemical calculations show that the emitting triplet excited state of persulfurated benzene derivatives involves excitations mostly localized on the central benzene core. The considered crystal structures indicate remarkably large distances between the persulfurated benzene cores of neighbor

© 2024 The Author(s). Chemistry - A European Journal published by Wiley-VCH GmbH

15213765, 2024, 43, Downloaded from https://chemistry-europe.onlinelibrary.wiley.com/doi/10.1002/chem.202401768 by Area Sistemi Dipart & Doc, Wiley Online Library on [25/03/2025]. See the Terms and Conditions (https://onlinelibrary.wiley.com/terms-and-conditions) on Wiley Online Library for rules of use; OA articles are governed by the applicable Creative Commons License

molecules, suggesting that excitonic interactions are not relevant; in addition, the out-of-plane deformations of persulfurated benzene cores found in the crystals are similar to the equilibrium structures computed for the isolated molecules (see Table 1). All the above factors point to a limited effect of the crystal environment on the molecular structure of the persulfurated benzene derivatives investigated here.

The amorphous phase is however disordered, with likely different environmental effects that we sought to elucidate with molecular dynamics simulations. We modelled the effects of the condensed phase on the excited states of **A6-Ph** using a multiscale hybrid approach based on molecular dynamics (MD) simulations in conjunction with TDDFT calculations (see details in the SI). Two representative snapshots taken from equilibrated MD simulations of the crystal at 300 K and of the amorphous phase at 80 K are shown in Figure 8. In the first case the environment keeps a relatively ordered structure (Figure 8a), when compared to the disorder typical of the amorphous phase in Figure 8b. With respect to gas phase calculations, the single-point TDDFT calculations carried out for different snapshots of the MD simulations show a stabilization of the lowest nπ* triplet state both in the simulated crystal at RT and in the simulated amorphous material at 80 K, with the latter environment inducing, however, a more remarkable decrease of the excitation energies (Table S6, SI; from 3.59 eV in gas phase to 3.20 eV in the equilibrated crystal at 300 K, to 3.03 eV in the amorphous material), in agreement with the observed red-shifted emission.

To better clarify the origin of the computed red shift, TDDFT calculations were also carried out on isolated molecules with the same geometry determined in the MD snapshots. The modest differences on excitation energies (ca. 0.02 eV) computed with or without the environment, can be ascribed to the electrostatic embedding induced by surrounding molecules. Thus, the dominant effect determining the red shift of ca. 0.17 eV on the T_1-S_0 transition in the amorphous environment, compared to the crystalline phase, must be attributed to different structural factors for the molecules embedded in the two environments, rather than to different electrostatic interactions.

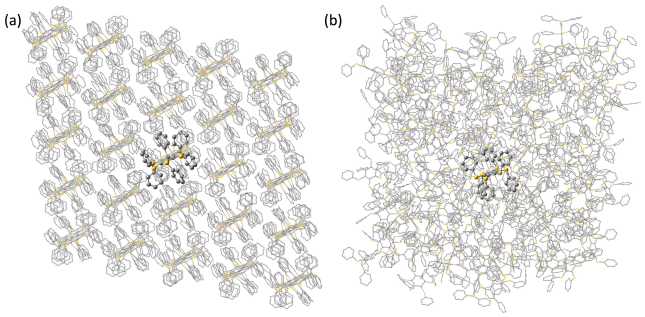

Figure 8. Examples of snapshots of the simulation cell containing **A6-Ph** molecules extracted from MD simulations for a) the crystalline phase at RT and b) for the amorphous phase at 80 K. The central molecule selected for the single point TDDFT calculations is visualized with ball and sticks graphics in both cases.

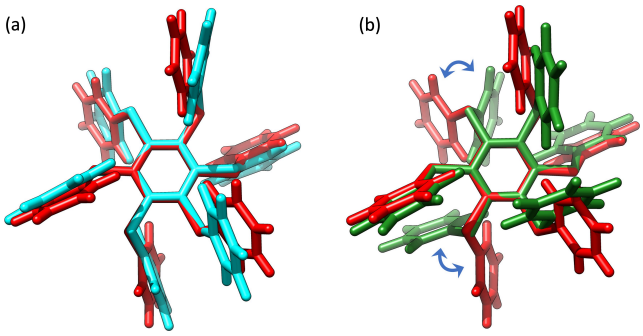

Figure 9. Superposition of a **A6-Ph** molecule taken from the crystal structure (red) with a molecule taken from a snapshot of MD simulations: (a) the cyan molecule from MD of the crystal at RT and (b) the green molecule from the MD of the amorphous phase at 80 K. The blue arrows indicate two remarkably different torsional angles around S–$C_{central}$ bonds for the red and green molecular structures.

To gain a deeper understanding of these differences, we superpose the molecular geometry derived from a snapshot of the MD simulation with that of a molecule within the crystalline structure. This is shown in Figure 9a for the MD carried out in the crystal at RT and Figure 9b for the simulation of the amorphous phase at 80 K. The cyan molecule in Figure 9a overlaps well with the red molecule taken from the crystal structure and shows very modest differences in twisting around S–$C_{central}$ bonds. The largest differences are detected for CSC angles and for rotations around S–C_{aryl} bonds. In contrast, the green molecule in Figure 9b, taken from the amorphous phase, apart from different rotations around S-C_{aryl} bonds, displays remarkably different rotation angles around some S–$C_{central}$ bonds (specifically those indicated by the blue arrows). Note that the conformation of the central persulfurated benzene remains *ababab*, but with some S–$C_{central}$ bond twisting that strongly deviates from those found in the crystal structure or determined by DFT geometry optimization.

We can summarize the above structural differences by stating that in the amorphous phase distorted *ababab* conformers (compared to the crystalline phase) can be found and are deemed to be responsible for the computed red shift of the T_1-S_0 transition.

Due to the small free volume available both in the crystalline and amorphous phases, the conversion between conformers of **A6**-derivatives (for instance from *ababab* to *aaabab*) is hampered and only distortions of the same conformer are detected in MD simulations of the amorphous phase. This would also explain why the amorphous phase returns to its initial crystal configuration upon heating from liquid N_2 temperature to RT.

Conclusions

Due to their structural flexibility, the emissive properties of persulfurated benzenes are crucially dependent on a combination of structural and constitutional factors. In this work, we have correlated structural and photophysical analyses, corrobo-

© 2024 The Author(s). Chemistry - A European Journal published by Wiley-VCH GmbH

15213765, 2024, 43, Downloaded from https://chemistry-europe.onlinelibrary.wiley.com/doi/10.1002/chem.202401768 by Area Sistemi Dipart & Doc, Wiley Online Library on [25/03/2025]. See the Terms and Conditions (https://onlinelibrary.wiley.com/terms-and-conditions) on Wiley Online Library for rules of use; OA articles are governed by the applicable Creative Commons License

15213765, 2024, 43, Downloaded from https://chemistry-europe.onlinelibrary.wiley.com/doi/10.1002/chem.202401768 by Area Sistemi Dipart & Doc, Wiley Online Library on [25/03/2025]. See the Terms and Conditions (https://onlinelibrary.wiley.com/terms-and-conditions) on Wiley Online Library for rules of use; OA articles are governed by the applicable Creative Commons License

rated by quantum-chemical calculations and MD simulations. The results presented lead to a comprehensive picture of the nature and the fate of the excited states available for this class of compounds, which represent important parameters to take into account for the design of solid-state functional materials based on the persulfurated benzene platform.

From these investigations key constitutional elements arise: *i*) for the alkyl-substituted persulfurated core (**B6-iPr**), the relaxation of the triplet excited state does not result in RT luminescence. This is mostly due to the high degree of structural disorder induced by intramolecular motions combined with the evidence, from calculations, of a CI seam between T_1 and S_0; *ii*) aryl-derivatives **A6**- in the solid state display phosphorescence emission at RT, whose energy is not significantly dependent on the presence or position of peripheral alkyl substituents; *iii*) crystalline solids of **A6**- derivatives are likely to emit from triplet states localized on individual molecules.

On the other hand, conformation-related factors can significantly modify the photophysical performance of **A6**-derivatives: *i*) each conformer can induce, with different efficiency, radiative or non-radiative deactivation of the T_1 excited state, as a consequence of its orbital nature and different SOC values for T_1-S_0 and/or available T_1-S_0 crossing; *ii)* according to MD simulations the free volume available in the condensed phase does not allow interconversion between conformers around the central persulfurated benzene; *iii*) in contrast to crystalline phases, the amorphous phases are likely to accentuate structural deformations, with red-shifted emission profiles at low temperature that reflect high geometrical constraints leading to highly distorted conformers, as evidenced by MD simulations.

Therefore, our approach validates the individuation of the best performing organic solid-state emitters based on the discrimination among the several conformers obtained both in crystalline and amorphous phases, each one displaying a specific excited-state landscape.

Supporting Information

The Supporting Information include synthetic procedures, details for XRD and structural analyses (Deposition Numbers 2330031 for **B6-iPr** at 300 K, 2330032 for **B6-iPr** at 110 K, 2330033 for **A6-iPr** contain the supplementary crystallographic data for this paper; these data are provided free of charge by the joint Cambridge Crystallographic Data Centre and Fachinformationszentrum Karlsruhe Access Structures service), supporting photophysical characterization and computational details.

Acknowledgements

Dr. Katia Rubini and Dr. Stefano Cerini (University of Bologna) are kindly acknowledged for assistance with the DSC experiments. FN acknowledges support by the European Union – Next Generation EU under the Italian National Recovery and Resilience Plan (PNRR M4 C2, Investimento 1.4 – Avviso n. 3138 del 16/12/2021 – CN00000013 National Centre for HPC, Big Data and Quantum Computing – CUP J33C22001170001). AF and PC thank the European Union, Programme NextGeneration EU, for the financial support of the project PNRR M4, C2, I1.4 Ecosystem for Sustainable Transition in Emilia-Romagna (ECOSISTER). MG is extremely grateful to the Agence Nationale de la Recherche (ANR) in France (PRC program) for the grant ANR-20-CE07-0031 Acronym: "SulfurDance". MG also acknowledge financial support from the Excellence Initiative of Aix-Marseille University – A*Midex, a French ''Investissements d'Avenir'' programme. A CNRS Program for International Scientific Collaborations (PICS 07573) with the University of Bologna is thanked, as well as Aix-Marseille Université, CINaM and CNRS France. Open Access publishing facilitated by Università degli Studi di Bologna, as part of the Wiley - CRUI-CARE agreement.

Conflict of Interests

The authors declare no conflict of interest.

Data Availability Statement

The data that support the findings of this study are available from the corresponding author upon reasonable request.

Keywords: room-temperature phosphorescence · organic phosphors · crystallization-induced emission · amorphization · TDDFT calculations

[1] W. Zhao, Z. He, B. Z. Tang, *Nat. Rev. Mater.* **2020**, *5*, 869–885.
[2] L. Ravotto, P. Ceroni, *Coord. Chem. Rev.* **2017**, *346*, 62–76.
[3] Z. Zhao, H. Zhang, J. W. Y. Lam, B. Z. Tang, *Angew. Chem. Int. Ed.* **2020**, *59*, 9888–9907.
[4] X. Cai, B. Liu, *Angew. Chem. Int. Ed.* **2020**, *59*, 9868–9886.
[5] I. Partanen, O. Al-Saedy, T. Eskelinen, A. J. Karttunen, J. J. Saarinen, O. Mrózek, A. Steffen, A. Belyaev, P. Chou, I. O. Koshevoy, *Angew. Chem.* **2023**, *135*, e202305108.
[6] M. S. Kwon, D. Lee, S. Seo, J. Jung, J. Kim, *Angew. Chem.* **2014**, *126*, 11359–11363.
[7] R. Boonsin, G. Chadeyron, J.-P. Roblin, D. Boyer, R. Mahiou, *J. Mater. Chem. C* **2015**, *3*, 9580–9587.
[8] W. Zhao, Z. He, J. W. Y. Lam, Q. Peng, H. Ma, Z. Shuai, G. Bai, J. Hao, B. Z. Tang, *Chem* **2016**, *1*, 592–602.
[9] H. Shi, Z. An, P.-Z. Li, J. Yin, G. Xing, T. He, H. Chen, J. Wang, H. Sun, W. Huang, Y. Zhao, *Cryst. Growth Des.* **2016**, *16*, 808–813.
[10] W. Shao, H. Jiang, R. Ansari, P. M. Zimmerman, J. Kim, *Chem. Sci.* **2022**, *13*, 789–797.
[11] S. Hirata, K. Totani, J. Zhang, T. Yamashita, H. Kaji, S. R. Marder, T. Watanabe, C. Adachi, *Adv. Funct. Mater.* **2013**, *23*, 3386–3397.
[12] M. S. Kwon, Y. Yu, C. Coburn, A. W. Phillips, K. Chung, A. Shanker, J. Jung, G. Kim, K. Pipe, S. R. Forrest, J. H. Youk, J. Gierschner, J. Kim, *Nat. Commun.* **2015**, *6*, 8947.
[13] Y. Chen, J. W. Y. Lam, R. T. K. Kwok, B. Liu, B. Z. Tang, *Mater. Horiz.* **2019**, *6*, 428–433.
[14] F. Würthner, *Angew. Chem. Int. Ed.* **2020**, *59*, 14192–14196.
[15] S. G. R. M. Pandey, A. S. J. Chakravarthy, *Mater. Chem. Front.* **2021**, *5*, 1541–1584.
[16] M. Villa, P. Ceroni, A. Fermi, *ChemPlusChem* **2022**, *87*, e202100558.

© 2024 The Author(s). Chemistry - A European Journal published by Wiley-VCH GmbH

[17] H. Zhang, X. Zheng, N. Xie, Z. He, J. Liu, N. L. C. Leung, Y. Niu, X. Huang, K. S. Wong, R. T. K. Kwok, H. H. Y. Sung, I. D. Williams, A. Qin, J. W. Y. Lam, B. Z. Tang, *J. Am. Chem. Soc.* **2017**, *139*, 16264–16272.
[18] L. Stojanović, R. Crespo-Otero, *ChemPhotoChem* **2019**, *3*, 907–915.
[19] J. Sturala, M. K. Etherington, A. N. Bismillah, H. F. Higginbotham, W. Trewby, J. A. Aguilar, E. H. C. Bromley, A.-J. Avestro, A. P. Monkman, P. R. McGonigal, *J. Am. Chem. Soc.* **2017**, *139*, 17882–17889.
[20] A. N. Sussardi, G. F. Turner, J. G. Richardson, M. A. Spackman, A. T. Turley, P. R. McGonigal, A. C. Jones, S. A. Moggach, *J. Am. Chem. Soc.* **2023**, *145*, 19780–19789.
[21] T. Kosaka, S. Iwai, Y. Inoue, T. Moriuchi, T. Mori, *J. Phys. Chem. A* **2018**, *122*, 7455–7463.
[22] J. Chen, C. C. W. Law, J. W. Y. Lam, Y. Dong, S. M. F. Lo, I. D. Williams, D. Zhu, B. Z. Tang, *Chem. Mater.* **2003**, *15*, 1535–1546.
[23] Z. Gan, Y. Liu, L. Wang, S. Jiang, N. Xia, Z. Yan, X. Wu, J. Zhang, W. Gu, L. He, J. Dong, X. Ma, J. Kim, Z. Wu, Y. Xu, Y. Li, Z. Wu, *Nat. Commun.* **2020**, *11*, 5572.
[24] Z. He, L. Zhang, J. Mei, T. Zhang, J. W. Y. Lam, Z. Shuai, Y. Q. Dong, B. Z. Tang, *Chem. Mater.* **2015**, *27*, 6601–6607.
[25] X. Ma, J. Wang, H. Tian, *Acc. Chem. Res.* **2019**, *52*, 738–748.
[26] J. Gierschner, J. Shi, B. Milián-Medina, D. Roca-Sanjuán, S. Varghese, S. Park, *Adv. Opt. Mater.* **2021**, *9*, 2002251.
[27] Z. Mao, Z. Yang, Y. Mu, Y. Zhang, Y. Wang, Z. Chi, C. Lo, S. Liu, A. Lien, J. Xu, *Angew. Chem. Int. Ed.* **2015**, *54*, 6270–6273.
[28] J. Zhang, M. Zhu, Y. Lu, X. Zhang, S. Xiao, H. Lan, T. Yi, *Chem. Eur. J.* **2022**, *28*, e202200458.
[29] Y. Tani, M. Terasaki, M. Komura, T. Ogawa, *J. Mater. Chem. C* **2019**, *7*, 11926–11931.
[30] M. Komura, T. Ogawa, Y. Tani, *Chem. Sci.* **2021**, *12*, 14363–14368.
[31] X. Cai, Z. Qiao, M. Li, X. Wu, Y. He, X. Jiang, Y. Cao, S. J. Su, *Angew. Chem. Int. Ed.* **2019**, *58*, 13522–13531.
[32] Z. Chen, X. Chen, D. Ma, Z. Mao, J. Zhao, Z. Chi, *J. Am. Chem. Soc.* **2023**, *145*, 16748–16759.
[33] J. Wei, C. Liu, J. Duan, A. Shao, J. Li, J. Li, W. Gu, Z. Li, S. Liu, Y. Ma, W. Huang, Q. Zhao, *Nat. Commun.* **2023**, *14*, 627.
[34] H. Qian, M. E. Cousins, E. H. Horak, A. Wakefield, M. D. Liptak, I. Aprahamian, *Nat. Chem.* **2017**, *9*, 83–87.
[35] J. Yang, X. Zhen, B. Wang, X. Gao, Z. Ren, J. Wang, Y. Xie, J. Li, Q. Peng, K. Pu, Z. Li, *Nat. Commun.* **2018**, *9*, 840.
[36] A. Huber, J. Dubbert, T. D. Scherz, J. Voskuhl, *Chem. Eur. J.* **2023**, *29*, e202202481.
[37] G. Bergamini, A. Fermi, C. Botta, U. Giovanella, S. Di Motta, F. Negri, R. Peresutti, M. Gingras, P. Ceroni, *J. Mater. Chem. C* **2013**, *1*, 2717–2724.
[38] A. Fermi, G. Bergamini, M. Roy, M. Gingras, P. Ceroni, *J. Am. Chem. Soc.* **2014**, *136*, 6395–6400.
[39] M. Villa, M. Roy, G. Bergamini, M. Gingras, P. Ceroni, *Dalton Trans.* **2019**, *48*, 3815–3818.
[40] X. Jia, C. Shao, X. Bai, Q. Zhou, B. Wu, L. Wang, B. Yue, H. Zhu, L. Zhu, *Proc. Nat. Acad. Sci.* **2019**, *116*, 4816–4821.
[41] M. Gingras, J. Raimundo, Y. M. Chabre, *Angew. Chem. Int. Ed.* **2006**, *45*, 1686–1712.
[42] A. Fermi, G. Bergamini, R. Peresutti, E. Marchi, M. Roy, P. Ceroni, M. Gingras, *Dyes Pigm.* **2014**, *110*, 113–122.
[43] H. Wu, G. V. Baryshnikov, A. Kuklin, B. F. Minaev, B. Wu, L. Gu, L. Zhu, H. Ågren, Y. Zhao, *ACS Appl. Mater. Interfaces* **2021**, *13*, 1314–1322.
[44] H. Wu, P. Zhao, X. Li, W. Chen, H. Ågren, Q. Zhang, L. Zhu, *ACS Appl. Mater. Interfaces* **2017**, *9*, 3865–3872.
[45] S. Riebe, C. Vallet, F. van der Vight, D. Gonzalez-Abradelo, C. Wölper, C. A. Strassert, G. Jansen, S. Knauer, J. Voskuhl, *Chem. Eur. J.* **2017**, *23*, 13660–13668.
[46] J. Stelzer, C. Vallet, A. Sowa, D. Gonzalez-Abradelo, S. Riebe, C. G. Daniliuc, M. Ehlers, C. A. Strassert, S. K. Knauer, J. Voskuhl, *ChemistrySelect* **2018**, *3*, 985–991.
[47] H. Wu, W. Chi, G. Baryshnikov, B. Wu, Y. Gong, D. Zheng, X. Li, Y. Zhao, X. Liu, H. Ågren, L. Zhu, *Angew. Chem. Int. Ed.* **2019**, *58*, 4328–4333.
[48] S. Shen, G. Baryshnikov, B. Yue, B. Wu, X. Li, M. Zhang, H. Ågren, L. Zhu, *J. Mater. Chem. C* **2021**, *9*, 11707–11714.
[49] S. Shen, G. V. Baryshnikov, Q. Xie, B. Wu, M. Lv, H. Sun, Z. Li, H. Ågren, J. Chen, L. Zhu, *Chem. Sci.* **2023**, *14*, 970–978.
[50] A. D. U. Hardy, D. D. MacNicol, D. R. Wilson, *J. Chem. Soc. Perkin Trans. 2* **1979**, *7*, 1011–1019.
[51] J. H. R. Tucker, M. Gingras, H. Brand, J.-M. Lehn, *J. Chem. Soc. Perkin Trans. 2* **1997**, 1303–1308.
[52] D. B. Werz, J. H. Schulte, R. Gleiter, F. Rominger, *J. Organomet. Chem.* **2004**, *689*, 3132–3142.
[53] D. Braga, S. D'Agostino, F. Grepioni, *Organometallics* **2012**, *31*, 1688–1695.
[54] P. Müller, in *Cryst. Struct. Refinement*, Oxford University Press, **2006**, pp. 56–96.
[55] M. Wrighton, D. L. Morse, *J. Am. Chem. Soc.* **1974**, *96*, 998–1003.
[56] F. Barigelletti, A. Juris, V. Balzani, P. Belser, A. Von Zelewsky, *J. Phys. Chem.* **1987**, *91*, 1095–1098.

Manuscript received: May 6, 2024
Accepted manuscript online: May 31, 2024
Version of record online: July 11, 2024

© 2024 The Author(s). Chemistry - A European Journal published by Wiley-VCH GmbH

15213765, 2024, 43, Downloaded from https://chemistry-europe.onlinelibrary.wiley.com/doi/10.1002/chem.202401768 by Area Sistemi Dipart & Doc, Wiley Online Library on [25/03/2025]. See the Terms and Conditions (https://onlinelibrary.wiley.com/terms-and-conditions) on Wiley Online Library for rules of use; OA articles are governed by the applicable Creative Commons License